# Supplementary Information

# Direct evidence for ligand-enhanced activity of Cu(I) sites

*Elvira Gouatieu Dongmo*[+,1,2] *Shabnam Haque*[+,1] *Florian Kreuter,*[1] *Toshiki Wulf,*[1,3] *Jiaye Jin,**[1] *Ralf Tonner-Zech,**[1] *Thomas Heine,*[*,2,3,4] *and Knut R. Asmis**[1]

*1) Wilhelm-Ostwald-Institut für Physikalische und Theoretische Chemie, Universität Leipzig, Linnéstr. 2, 04103 Leipzig, Germany*

*2) Institute of Resource Ecology, Research Site Leipzig, Helmholtz-Zentrum Dresden-Rossendorf, Permoserstr. 15, 04318 Leipzig, Germany*

*3) Faculty of Chemistry and Food Chemistry, School of Science, TU Dresden, 01062 Dresden, Germany*

*4) Department of Chemistry and ibs for nanomedicine, Yonsei University, Seodaemun-gu, Seoul 120-749, Republic of Korea*

*Electronic mail: jiaye.jin@uni-leipzig.de, ralf.tonner@uni-leipzig.de, thomas.heine@tu-dresden.de, knut.asmis@uni-leipzig.de*

## Table of contents

## TOF mass spectra

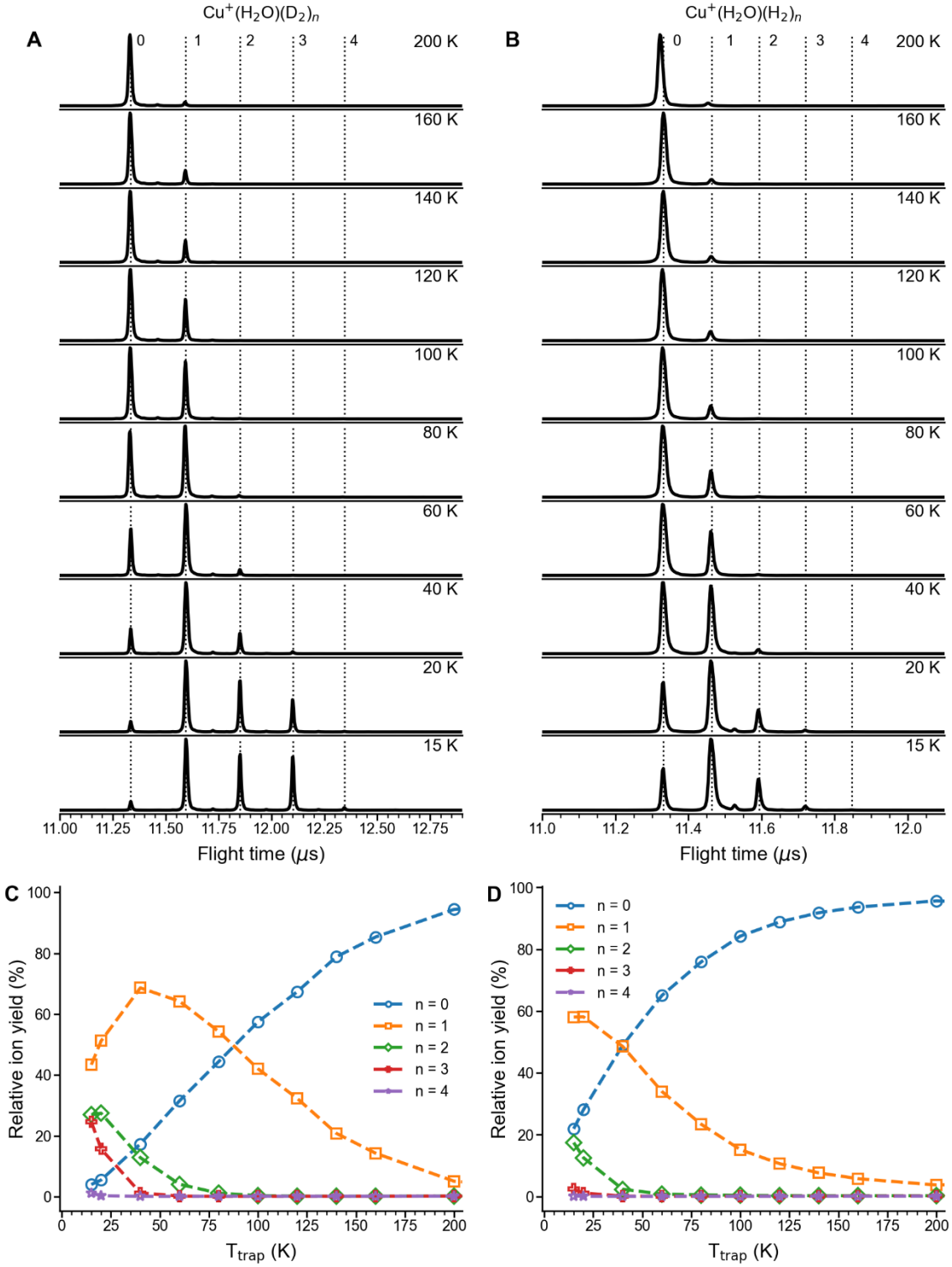


**Figure S1**: TOF mass spectra of (A) $Cu^+(H_2O)(D_2)_n$ and (B) $Cu^+(H_2O)(H_2)_n$ obtained after storing $Cu^+(H_2O)$ on average 50 ms in the ion trap (filled with around 1 mbar $D_2$ or $H_2$) for different ion-trap temperatures. Relative ion yield of (C) $Cu^+(H_2O)(D_2)_n$ and (D) $Cu^+(H_2O)(H_2)_n$.

## IRPD spectra

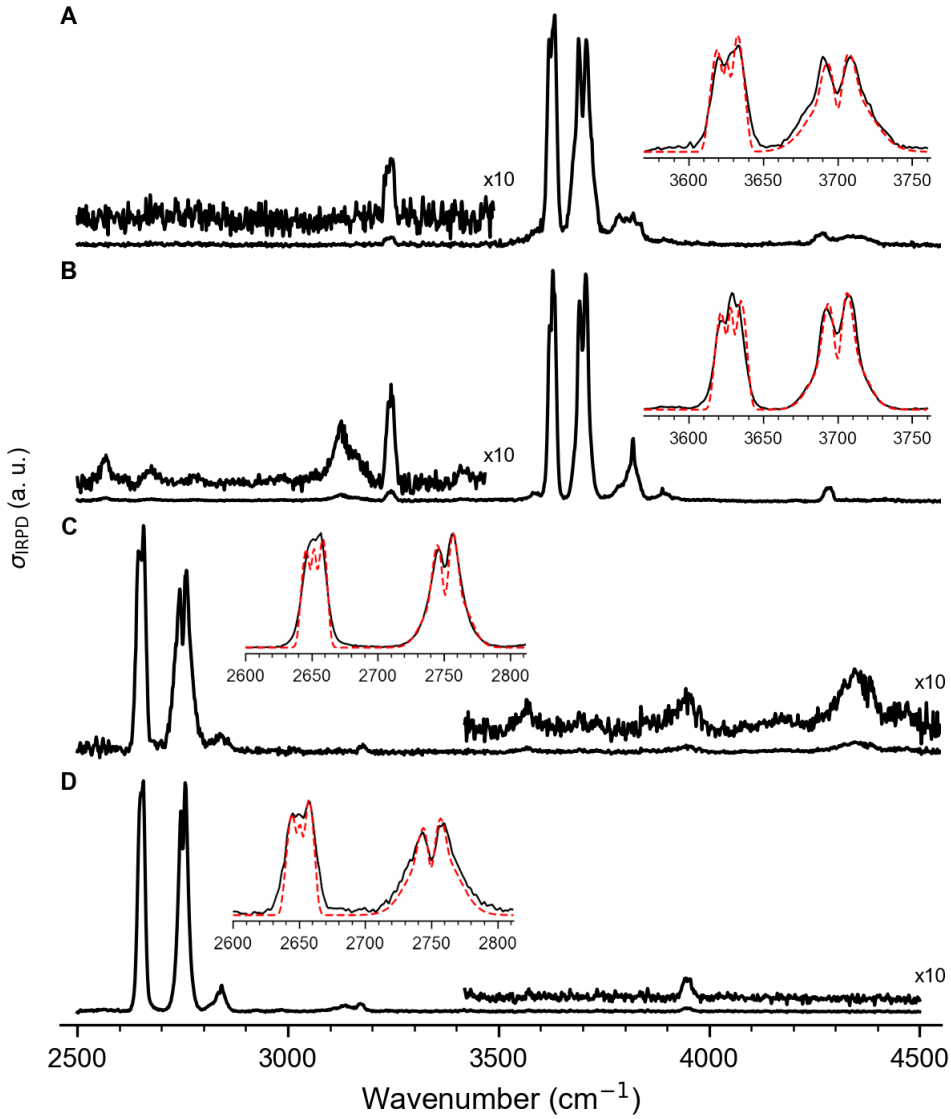


**Figure S2**: IRPD spectra of $Cu^+(H_2O)(H_2)_2$ and its isotopologues. A) $Cu^+(H_2O)(H_2)_2$, B) $Cu^+(H_2O)(D_2)_2$, C) $Cu^+(D_2O)(H_2)_2$, and D) $Cu^+(D_2O)(D_2)_2$. The spectra are magnified for showing the rovibrational profiles of OH/OD stretching bands. The rotational constants calculated using VPT2/MP2/def2-TZVPP (see following calculation results) are applied to fit the $\nu^{s}_{OH/D}$ and $\nu^{as}_{OH/D}$ frequencies, which are simulated at 100 K temperature and with 4.5 $cm^{-1}$ width for the Gaussian lineshape profile, using the PGOPHER program.[36] The standard deviations of the fitting frequencies are 0.3 – 0.5 $cm^{-1}$.

## Supplementary Note 1: Validation

Our calculations show that MP2/def2-TZVPP structures and harmonic frequencies (see **Table S3, Table S4** and **Figure S4**) match the CCSD(T)/aug-cc-pVTZ(-PP) ones very closely. Hence, MP2/def2-TZVPP appears to be a sufficient level of theory for the computation of anharmonic frequencies of $Cu^+(H_2O)(H_2)_2$ and its isotopoloues. The ZPE-corrected bond dissociation energy (BDE, $D_0$) of $Cu^+(H_2O)$ obtained using MP2/def2-TZVPP and CCSD(T)/aug-cc-pVTZ(-PP) calculations is 157 and 161 $kJ \cdot mol^{-1}$, respectively. This is in agreement with the experimental value (157 $kJ \cdot mol^{-1}$) reported by Paul R. Kemper *et al.*[14] and by previous MP2 and CCSD(T) calculations.[15,19] The calculated vibrational frequencies of $H_2O$ and $Cu^+(H_2O)$ isotopologues are reported in **Table S7**.

**Table S3.** Bond lengths and angles according to CCSD(T)/aug-cc-pVTZ(-PP) (in parentheses: MP2/def2-TZVPP) calculations. Structures are shown in **Figure 3.** All interatomic distances are given in Angstrom (Å) and angles in degrees (°).

| | Symmetry | r(Cu-O) | r(O-H) | r(Cu-$H_2$) | r(H-H) | ∠(H-O-Cu) | ∠( H-O-H) |
|---|---|---|---|---|---|---|---|
| **$H_2$** | $C_{2v}$ | | | | 0.743(0.737) | | |
| **$H_2O$** | $C_{2v}$ | / | 0.962(0.958) | / | / | / | 104.2 (103.8) |
| **$Cu^+(H_2)$** | $C_{2v}$ | / | / | 1.754(1.644) | 0.763(0.780) | / | / |
| **$Cu^+(H_2O)$** | $C_{2v}$ | 1.935 (1.931) | 0.929 (0.963) | / | / | 127.61 (126.47) | 104.8 (107.1) |
| **$Cu^+(H_2O)(H_2)$** | $C_{2v}$ | 1.881(1.875) | 0.965 (0.963) | 1.579 (1.549) | 0.796 (0.796) | 125.97 (125.92) | 108.0 (107.8) |
| **$Cu^+(H_2O)(H_2)_2$** | $C_{2v}$ | 1.948 (1.947) | 0.964 (0.963) | 1.642 (1.651) | 0.790 (0.789) | 126.40 (126.53) | 107.1 (106.9) |
| **$Cu^+(H_2O)(H_2)_3$** | $C_{2v}$ | (2.069) | (0.962) | (1.720) | (0.778) | (126.92) | (106.2) |

**Table S4.** Geometrical parameters of $Cu^+(H_2O)(H_2)_2$ at different computational levels. Distances in Angstroms (Å), angles and dihedral angles in degree (°), the numbering of the atoms is given in **Figure S4.**

| Parameters | CCSD(T)/ aug-cc-pVTZ (-PP) [ CCSD(T)/aug-cc-pVTZ] | MP2/ def2-TZVPP | **MP2/ aug-cc- pVTZ (-PP)** [ MP2/aug-cc- pVTZ] |
|---|---|---|---|
| r(Cu-O) | 1.948 [1.971] | 1.947 | 1.914 [1.938] |
| r(Cu-X1/X2) | 1.642 [1.695] | 1.651 | 1.591 [1.675] |
| r(O-H1/H2) | 0.964 [0.964] | 0.963 | 0.965 [0.965] |
| r(H3-H4) | 0.790 [0.782] | 0.789 | 0.802 [0.7901] |
| ∠(H1-O-H2) | 107.15 [106.90] | 106.93 | 107.26 [106.94] |
| ∠(H2-O-Cu) | 126.43 [126.55] | 126.53 | 126.37 [126.53] |
| ∠(X1/X2-Cu-O) | 120.64 [121.12] | 119.98 | 120.04 [119.05] |

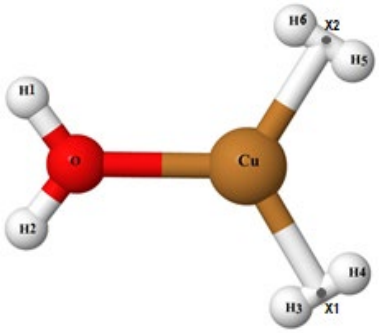


**Figure S4.** Optimized geometry of $Cu^+(H_2O)(H_2)_2$ at the CCSD(T)/aug-cc-pVTZ(-PP) level and definition of geometry parameters. X1 and X2 represent the centers of mass of $H_2$ ligands.

## Supplementary Note 2: Influence of relativistic effects

The interatomic distances around the $Cu^+$ are substantially influenced by relativistic effects. CCSD(T) in combination with aug-cc-pVTZ(-PP), which includes relativistic effects implicitly via the effective core potentials (ECP), yields Cu–$H_2$ and Cu–O bonds that are respectively shorter by 3.4 pm and 2.1 pm than those calculated employing the respective all-electron basis set (see Table S4). This leads to a blue-shift of the corresponding stretching frequencies, elongation of the H–H bonds and a red-shift of the H–H stretching frequency. That this is a result of relativistic effects is corroborated by the fact that a comparison between non-relativistic DFT calculations and ones including relativistic effects employing the zeroth-order regular approximation (ZORA) yields similar results (see **Table S5**; calculations performed with AMS version 2022.104). MP2 in combination with the aug-cc-pVTZ(-PP) basis set yields even shorter bonds with commensurate effects on the respective vibrational frequencies. This is likely due to the known tendency of MP2 to overestimate London dispersion – an effect that may, to some extent, be cured by the use of a moderately sized basis set that is too small to capture the full strength of the partially spurious MP2 dispersion. It is likely for this reason that (as shown in **Table S6**) MP2 in combination with the moderately sized def2-TZVPP basis set gives bonds lengths and harmonic frequencies very similar to the CCSD(T)/aug-cc-pVTZ(-PP) benchmark. The remarkably good agreement between the experimental vibrational spectra and the VPT2 spectra calculated on the MP2/def2-TZVPP potential energy surface, therefore, appears to be in part be due to error compensation, underscoring the importance of balancing method and basis set for hydrogen and the transition metal in such calculations.

**Table S5.** Harmonic vibrational frequencies for $Cu^+(H_2O)(H_2)_2$ (wavenumbers in $cm^{-1}$ and assignments) calculated using different method / basis sets combinations.

| Mode | PBE0/TZ 2P(Slater) | PBE0/TZ2P (Slater) +scalar | MP2/aug-cc-pVTZ | MP2/aug-cc-pVTZ(-PP) | MP2/def2 -TZVPP | CCSD(T)/aug-cc-pVTZ(-PP) | CCSD(T)/aug -cc-pVTZ | Mode description |
|---|---|---|---|---|---|---|---|---|
| 1 | 126 | 140 | 171 | 167 | 156 | 140 | 108 | HOH out-of-plane hindered rotation |
| 2 | 160 | 172 | 179 | 193 | 172 | 149 | 129 | $H_2CuH_2$ in-plane libration bend |
| 3 | 207 | 192 | 185 | 199 | 187 | 160 | 142 | HOH out-of-plane libration bend |
| 4 | 248 | 273 | 277 | 314 | 270 | 239 | 242 | $H_2CuH_2$ out-of-plane libration bend |
| 5 | 288 | 311 | 341 | 379 | 324 | 317 | 281 | H2-Cu-H2 bending |
| 6 | 337 | 373 | 410 | 454 | 394 | 347 | 323 | Sym. out-of-plane $H_2$ hindered rotation |
| 7 | 340 | 374 | 412 | 467 | 400 | 364 | 326 | Antisym. out-of-plane $H_2$ hindered rotation |
| 8 | 392 | 411 | 425 | 472 | 412 | 419 | 395 | Cu-O stretch |
| 9 | 569 | 583 | 595 | 615 | 591 | 584 | 565 | HOH in-plane libration bend |
| 10 | 804 | 859 | 897 | 976 | 880 | 877 | 790 | Antisym. Cu-$H_2$ stretch |
| 11 | 840 | 912 | 928 | 1037 | 918 | 1037 | 821 | Sym. Cu-$H_2$ stretch |
| 12 | 1185 | 1276 | 1366 | 1493 | 1310 | 1309 | 1178 | Antisym. Cu-$H_2$ stretch |

| | | | | | | | | |
|---|---|---|---|---|---|---|---|---|
| 13 | 1190 | 1281 | 1371 | 1500 | 1331 | 1311 | 1180 | Sym. Cu-$H_2$ stretch |
| 14 | 1652 | 1654 | 1671 | 1672 | 1681 | 1682 | 1681 | H-O-H bend |
| 15 | 3741 | 3645 | 3727 | 3571 | 3745 | 3720 | 3794 | Sym. HH stretch |
| 16 | 3753 | 3656 | 3737 | 3577 | 3754 | 3722 | 3832 | Antisym. HH stretch |
| 17 | 3817 | 3814 | 3780 | 3778 | 3809 | 3793 | 3835 | Sym. OH stretch |
| 18 | 3899 | 3895 | 3877 | 3874 | 3905 | 3877 | 3878 | Antisym. OH stretch |

**Table S6.** H–H distances (pm) and computed H–H stretch frequencies ($cm^{-1}$) at different levels of theory.

| | H–H distance in | | | | |
|---|---|---|---|---|---|
| | free $H_2$ | $Cu^+(H_2O)(H_2)$ | $Cu^+(H_2O)(H_2)_2$ | $\Delta_1$(ads) | $\Delta_2$(ads) |
| MP2/def2-TZVPP | 73.7 | 79.2 | 78.9 | 5.5 | 5.2 |
| MP2/aug-cc-pVTZ(-PP) | 73.7 | 80.4 | 78.9 | 6.7 | 5.2 |
| CCSD(T)/aug-cc-pVTZ(-PP) | 74.3 | 79.6 | 79.0 | 5.3 | 4.7 |

$\Delta_1$(ads) and $\Delta_2$(ads): difference between H–H distance in free $H_2$ and in $Cu^+(H_2O)(H_2)$ and in $Cu^+(H_2O)(H_2)_2$, respectively.

| | harmonic H–H stretching frequency in | | | | |
|---|---|---|---|---|---|
| | free $H_2$ | $Cu^+(H_2O)(H_2)$ | $Cu^+(H_2O)(H_2)_2$ | $\Delta_1$(ads) | $\Delta_2$(ads) |
| MP2/def2-TZVPP | 4526 | 3672 | 3745<br>3754 | -854 | -781<br>-772 |
| CCSD(T)/aug-cc-pVTZ(-PP) | 4401 | 3665 | 3720<br>3722 | -736 | -681<br>-679 |

| | VPT2 H–H stretching frequency in | | | | |
|---|---|---|---|---|---|
| | free $H_2$ | $Cu^+(H_2O)(H_2)$ | $Cu^+(H_2O)(H_2)_2$ | $\Delta_1$(ads) | $\Delta_2$(ads) |
| MP2/def2-TZVPP | 4298 | 3481 | 3565 | -817 | -733 |
| CCSD(T)/aug-cc-pVTZ(-PP) | 4146 | – | – | – | – |

$\Delta_1$(ads) and $\Delta_2$(ads): difference between the H–H stretching frequencies of free $H_2$ and $H_2$ adsorbed in $Cu^+(H_2O)(H_2)$ and $Cu^+(H_2O)(H_2)_2$, respectively.

| | | | | | |
|---|---|---|---|---|---|
| 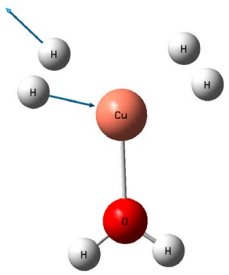 | 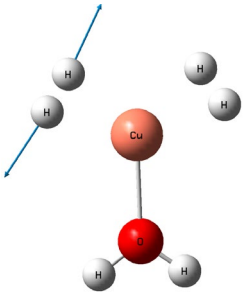 | 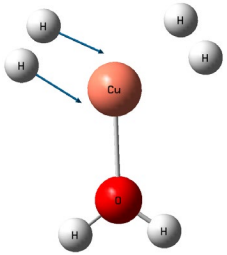 | 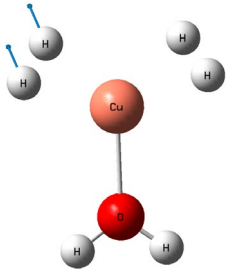 | 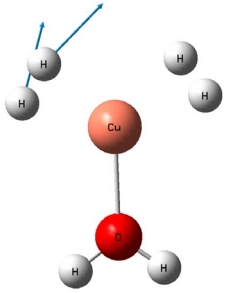 | 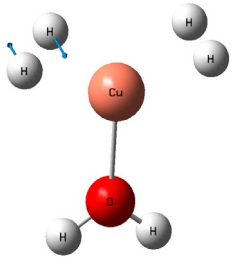 |
| $\upsilon_{HCuH}$ $(1307\ \mathrm{cm}^{-1})$<br>$\upsilon_{DCuD}$ $(926\ \mathrm{cm}^{-1})$<br>'Hindered translation' | $\nu_{H_2}(3754\ \mathrm{cm}^{-1})$<br>$\nu_{D_2}(2659\ \mathrm{cm}^{-1})$<br>'H-H vibration' | $\nu_{CuH_2}(871\ \mathrm{cm}^{-1})$<br>$\nu_{CuD_2}(617\ \mathrm{cm}^{-1})$<br>'$Cu^{+}$-$H_2$ vibration' | $\delta^{IP}_{CuH_2}(198\ \mathrm{cm}^{-1})$<br>$\delta^{IP}_{CuD_2}(140\ \mathrm{cm}^{-1})$<br>'Hindered rotation' | $\delta^{OOP}_{CuH_2}(280\ \mathrm{cm}^{-1})$<br>$\delta^{OOP}_{CuD_2}(198\ \mathrm{cm}^{-1})$<br>'Hindered translation' | $\tau^{OOP}_{H_2}(390\ cm^{-1})$<br>$\tau^{OOP}_{D_2}(276\ cm^{-1})$<br>'Rotation' |

**Figure S6**: The displacements and corresponding vibrational normal modes of the bound $H_2/D_2$ to the frozen $Cu^{+}(H_2O)(H_2)$ fragment. (two vibrations, two hindered translational modes and two hindered rotational mode).

**Table S8.** Calculated bond dissociation energy ($D_e$), for the reaction $Cu^+(H_2O)(H_2)_n \rightarrow Cu^+(H_2O)(H_2)_{n-1} + H_2$, ($n$=1,2). All values are in kJ·mol$^{-1}$ and from the bottom of the potential well on the PES, *i.e.* without ZPE correction (Born-Oppenheimer energies).

| | $Cu^+(H_2O)(H_2)$ | $Cu^+(H_2O)(H_2)_2$ |
|---|---|---|
| MP2/def2-TZVPP | 90.86 | 28.67 |
| MP2/aug-cc-pVTZ(-PP) | 112.29 | 30.96 |
| MP2/aug-cc-pVQZ(-PP) | 113.29 | 31.13 |
| CCSD(T)/aug-cc-pVTZ(-PP) | 96.33 | 27.71 |
| CCSD(T)/aug-cc-pVQZ(-PP)// CCSD(T)/aug-cc-pVTZ(-PP) | 97.23 | 29.14 |

Note: The calculated bond dissociation energy ($D_e$) at the CCSD(T)/aug-cc-pVQZ(-PP) level uses the geometry optimized at the CCSD(T)/ aug-cc-pVTZ(-PP) level.

**Table S9.** Expectation values <R> (in Å) of bond distance between Cu and the center of the adsorbed hydrogen isotopologues. $R_e$ = 1.6423 Å is the bond length obtained from fitting the data obtained at the CCSD(T)/aug-cc-pVTZ-(PP) level to the Morse.

.

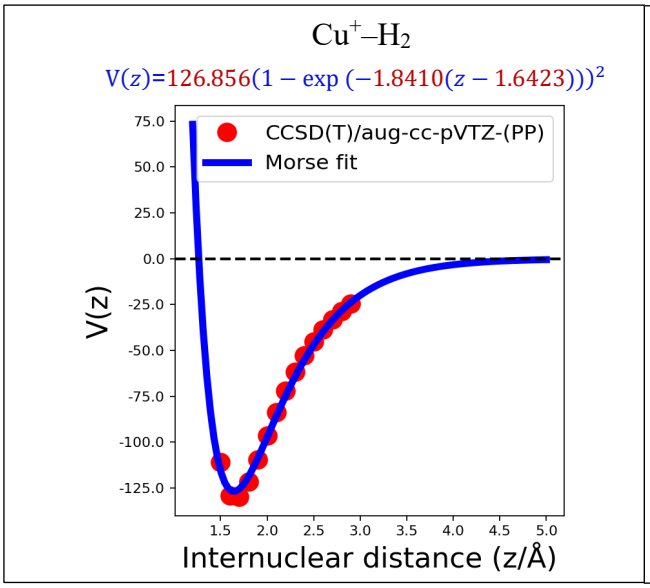


| | <R> (Å) | <R>-$R_e$ (Å) |
|---|---|---|
| **$H_2$** | 1.796 | 0.154 |
| **$D_2$** | 1.768 | 0.125 |
| **$T_2$** | 1.755 | 0.113 |
| **HD** | 1.779 | 0.137 |
| **HT** | 1.774 | 0.131 |
| **DT** | 1.761 | 0.119 |

**Table S10.** Expectation values <r> (in Å) of bond distance of adsorbed isotopologues. $r_e = 0.7904$ Å is the bond length obtained after fitting the data obtained at the CCSD(T)/aug-cc-pVTZ-(PP) level to the Morse.

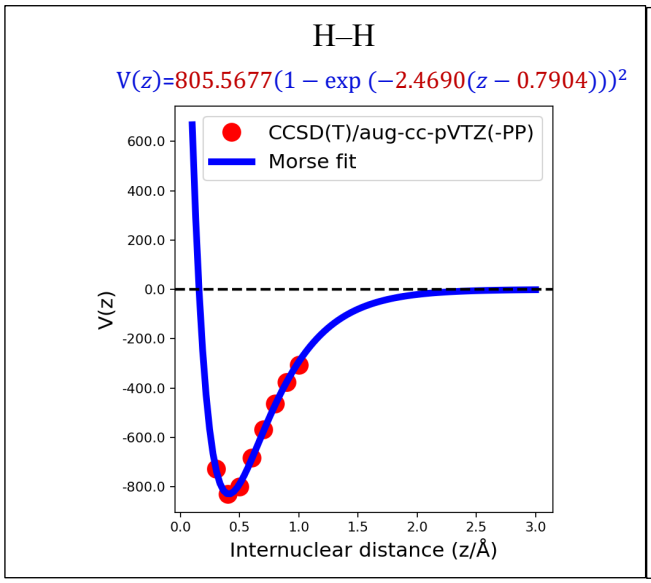


| | <r> (Å) | <r>-$r_e$ (Å) |
|---|---|---|
| **$H_2$** | 0.8076 | 0.0172 |
| **$D_2$** | 0.8020 | 0.0116 |
| **$T_2$** | 0.8009 | 0.0105 |
| **HD** | 0.8043 | 0.0139 |
| **HT** | 0.8035 | 0.0131 |
| **DT** | 0.8014 | 0.0110 |

**Table S11:** Predicted separation factors for dihydrogen isotopologue adsorption at $Cu^+$, $Cu^+(H_2O)(H_2)$, $Cu^+(H_2O)$ as a function of temperatures.

| $Cu^+(H_2O)(H_2)$ | | | | |
|---|---|---|---|---|
| **T(K)** | $\alpha(D_2/H_2)$ | $\alpha(HD/H_2)$ | $\alpha(DT/D_2)$ | $\alpha(T_2/D_2)$ |
| **80** | 43.77 | 8.10 | 2.06 | 3.82 |
| **90** | 25.64 | 6.00 | 1.83 | 3.06 |
| **100** | 16.78 | 4.74 | 1.66 | 2.60 |
| **110** | 11.91 | 3.91 | 1.54 | 2.23 |
| **120** | 8.98 | 3.34 | 1.45 | 1.99 |
| **130** | 7.08 | 2.93 | 1.38 | 1.81 |
| **140** | 5.79 | 2.62 | 1.32 | 1.67 |
| **150** | 4.88 | 2.38 | 1.27 | 1.56 |
| **160** | 4.20 | 2.19 | 1.23 | 1.47 |
| **170** | 3.69 | 2.04 | 1.20 | 1.40 |
| **180** | 3.29 | 1.91 | 1.17 | 1.34 |
| **200** | 2.71 | 1.72 | 1.13 | 1.24 |
| **220** | 2.33 | 1.58 | 1.09 | 1.18 |
| **240** | 2.05 | 1.47 | 1.07 | 1.12 |
| **260** | 1.85 | 1.39 | 1.05 | 1.08 |

| $Cu^+$ | | | |
|---|---|---|---|
| **T (K)** | $\alpha(D_2/H_2)$ | $\alpha(HD/H_2)$ | $\alpha(T_2/D_2)$ |
| **80** | 17.77 | 4.35 | 3.16 |
| **90** | 13.80 | 3.81 | 2.83 |
| **100** | 11.08 | 3.40 | 2.57 |
| **110** | 9.13 | 3.07 | 2.37 |
| **120** | 7.70 | 2.81 | 2.20 |
| **130** | 6.61 | 2.60 | 2.06 |
| **140** | 5.77 | 2.42 | 1.95 |
| **150** | 5.10 | 2.27 | 1.85 |
| **160** | 4.57 | 2.14 | 1.76 |
| **170** | 4.13 | 2.03 | 1.69 |
| **180** | 3.76 | 1.93 | 1.62 |
| **200** | 3.20 | 1.77 | 1.52 |
| **220** | 2.79 | 1.65 | 1.43 |
| **240** | 2.48 | 1.55 | 1.37 |
| **260** | 2.24 | 1.47 | 1.31 |

| $Cu^+(H_2O)(H_2)$ | | | | |
|---|---|---|---|---|
| **T (K)** | $\alpha(D_2/H_2)$ | $\alpha(HD/H_2)$ | $\alpha(DT/D_2)$ | $\alpha(T_2/D_2)$ |
| **80** | 15.53 | 4.48 | 1.62 | 2.44 |
| **90** | 10.35 | 3.56 | 1.48 | 2.06 |
| **100** | 7.50 | 2.97 | 1.38 | 1.81 |
| **110** | 5.77 | 2.56 | 1.30 | 1.63 |
| **120** | 4.64 | 2.27 | 1.24 | 1.49 |
| **130** | 3.87 | 1.04 | 1.19 | 1.39 |
| **140** | 3.32 | 1.87 | 1.15 | 1.31 |
| **150** | 2.91 | 1.74 | 1.12 | 1.24 |
| **160** | 2.59 | 1.63 | 1.09 | 1.19 |
| **170** | 2.35 | 1.54 | 1.07 | 1.15 |
| **180** | 2.15 | 1.47 | 1.05 | 1.11 |
| **200** | 1.86 | 1.35 | 1.02 | 1.06 |
| **220** | 1.66 | 1.27 | 1.00 | 1.02 |
| **230** | 1.58 | 1.23 | 0.99 | 1.00 |
| **240** | 1.51 | 1.20 | 0.98 | 0.99 |
| **260** | 1.41 | 1.15 | 0.97 | 0.97 |

| $Cu^+(H_2O)$ | | | |
|---|---|---|---|
| **T (K)** | $\alpha(D_2/H_2)$ | $\alpha(HD/H_2)$ | $\alpha(T_2/D_2)$ |
| **80** | 103.39 | 13.59 | 5.59 |
| **90** | 69.74 | 10.89 | 4.74 |
| **100** | 49.61 | 9.00 | 4.11 |
| **110** | 36.85 | 7.62 | 3.63 |
| **120** | 28.37 | 6.58 | 3.26 |
| **130** | 22.49 | 5.78 | 2.96 |
| **140** | 18.29 | 5.15 | 2.72 |
| **150** | 15.19 | 4.64 | 2.52 |
| **160** | 12.84 | 4.23 | 2.35 |
| **170** | 11.03 | 3.89 | 2.21 |
| **180** | 9.61 | 4.00 | 2.08 |
| **200** | 7.54 | 3.15 | 1.89 |
| **220** | 6.14 | 2.81 | 1.74 |
| **230** | 5.60 | 2.67 | 1.67 |
| **240** | 5.15 | 2.55 | 1.62 |
| **260** | 4.42 | 2.34 | 1.52 |

**Table S12.** Ground state rotational constants A, B and C (in $cm^{-1}$) of $Cu^+(H_2O)$ and $Cu^+(H_2O)(H_2)_2$ isotopologues.

| | harmonic CCSD(T)/aug-cc-pVTZ (-PP) | | |
|---|---|---|---|
| | A | B | C |
| $Cu^+(H_2O)$ | 14.095 | 0.297 | 0.292 |
| $Cu^+(H_2O)(H_2)$ | 10.889 | 0.272 | 0.269 |
| $Cu^+(H_2O)(H_2)_2$ | 1.796 | 0.263 | 0.229 |
| $Cu^+(H_2O)(D_2)_2$ | 0.961 | 0.240 | 0.192 |
| $Cu^+(D_2O)(H_2)_2$ | 1.591 | 0.231 | 0.202 |
| $Cu^+(D_2O)(D_2)_2$ | 0.899 | 0.212 | 0.171 |

| | VPT2 MP2/def2-TZVPP | | |
|---|---|---|---|
| | A | B | C |
| $Cu^+(H_2O)$ | 13.940 | 0.299 | 0.293 |
| $Cu^+(H_2O)(H_2)$ | 10.978 | 0.273 | 0.269 |
| $Cu^+(H_2O)(H_2)_2$ | 1.818 | 0.264 | 0.230 |
| $Cu^+(H_2O)(D_2)_2$ | 0.976 | 0.242 | 0.194 |
| $Cu^+(D_2O)(H_2)_2$ | 1.610 | 0.232 | 0.203 |
| $Cu^+(D_2O)(D_2)_2$ | 0.912 | 0.213 | 0.172 |

**Table S13.** $H_2$ isotopologue desorption energies (kJ·mol$^{-1}$) for the reaction $Cu^+(H_2O)(H_2)_2 \rightarrow Cu^+(H_2O)(H_2) + H_2$. ZPE corrections from the harmonic approximation.

| Species $C_{2V}$ symmetry | **$2H_2$ and isotopologues attached to $Cu^+(H_2O)$** | | | |
|---|---|---|---|---|
| | MP2/def2-TZVPP | MP2/aug-cc-pVTZ (-PP) | MP2/aug-cc-pVQZ (-PP) | CCSD(T)/aug-cc-pVTZ (-PP) |
| | $\Delta_{des}E(0K)$ | $\Delta_{des}E(0K)$ | $\Delta_{des}E(0K)$ | $\Delta_{des}E(0K)$ |
| $Cu^+(H_2O)(H_2)_2$ | 17.1 | 20.2 | 17.4 | 14.4 |
| $Cu^+(H_2O)(D_2)_2$ | 20.3 | 22.6 | 21.0 | 17.6 |
| $Cu^+(H_2O)(T_2)_2$ | 21.7 | 23.9 | 22.7 | 19.3 |
| $Cu^+(H_2O)(HD)_2$ | 18.8 | 21.4 | 19.4 | 15.8 |
| $Cu^+(H_2O)(HT)_2$ | 19.7 | 22.3 | 20.4 | 16.7 |
| $Cu^+(H_2O)(DT)_2$ | 21.0 | 23.3 | 22.0 | 18.4 |
| **$2H_2$ and isotopologues attached to $Cu^+(D_2O)$** | | | | |
| $Cu^+(D_2O)(H_2)_2$ | 17.3 | 20.4 | 17.8 | 14.3 |
| $Cu^+(D_2O)(D_2)_2$ | 20.4 | 22.9 | 21.5 | 18.0 |
| $Cu^+(D_2O)(T_2)_2$ | 21.8 | 24.3 | 23.1 | 19.6 |
| $Cu^+(D_2O)(HD)_2$ | 19.6 | 22.0 | 19.6 | 16.2 |
| $Cu^+(D_2O)(HT)_2$ | 20.3 | 22.7 | 20.8 | 17.2 |
| $Cu^+(D_2O)(DT)_2$ | 21.7 | 24.0 | 22.4 | 18.8 |
| **$2H_2$ and isotopologues attached to $Cu^+(T_2O)$** | | | | |
| $Cu^+(T_2O)(H_2)_2$ | 18.0 | 20.2 | 18.0 | 14.5 |
| $Cu^+(T_2O)(D_2)_2$ | 20.6 | 23.1 | 21.7 | 18.2 |
| $Cu^+(T_2O)(T_2)_2$ | 21.9 | 24.4 | 23.3 | 19.9 |
| $Cu^+(T_2O)(HD)_2$ | 19.7 | 22.0 | 20.0 | 16.4 |
| $Cu^+(T_2O)(HT)_2$ | 20.5 | 22.9 | 20.6 | 17.4 |
| $Cu^+(T_2O)(DT)_2$ | 21.8 | 24.2 | 22.4 | 19.0 |

The ZPEs of free hydrogen isotopologues, namely $H_2$, $D_2$, and $T_2$, are 26.3 kJ·mol$^{-1}$, 18.6 kJ·mol$^{-1}$, and 15.2 kJ·mol$^{-1}$, respectively.

## Energy decomposition analysis (EDA) of the $Cu^+$-$H_2$ bond

### XC-functional benchmark

To determine the appropriate setup for the DFT calculations, we benchmarked the Cu–$H_2$ bonding energy of complex $Cu(H_2O)(H_2)_2^+$ with different XC functionals against the CCSD(T). We selected a range of XC functionals, including LDA, GGA (BLYP[37], PBE[38]), meta-GGA (TPSS[39],

M06L[40,41]), hybrid (PBE0[42], B3LYP[32]), meta-hybrid (TPSSh[43], M06[40,41], M06-2x[40,41]), range separate hybrid (CAM-B3LYP[44], wB97X-D3[45], LC-BLYP[46]), and double hybrid (PWPB95[47], B2PLYP[48]). Grimme D3[49] dispersion correction was confidently employed for all functionals, and Grimme D4[50] dispersion correction was also confidently utilized for certain functionals. All calculations were performed using the ORCA 4.2.1 program package[51], including the DFT and CCSD(T) reference calculation. The basis set utilized was def2-TZVPP[52], and the RIJCOSX approximation was also employed. Therefore Def2/J was used as auxiliary basis set. The SCF energy convergence criterion was set to $10^{-8}$ $E_H$. The benchmark calculations utilized the geometry-optimized structure of $H_2$, fragment $Cu^+(H_2O)(H_2)$, and complex $Cu^+(H_2O)(H_2)_2$ at the PBE-D3/def2-TZVPP level. The results of the benchmark are presented in **Table S14** and **Figure S7**.

**Table S14**: Results of the benchmark study for Cu–$H_2$ bond in $Cu^+(H_2O)(H_2)_2$. All values given in kJ·mol$^{-1}$.

| Functional class | functional | $\Delta E_{bond}(Cu-H_2)$ | $\Delta E(DFT)-\Delta E(CCSD(T))$ |
|---|---|---|---|
| LDA | LDA-D3 | -68.2 | -41.5 |
| GGA | PBE-D3 | -39.1 | -12.4 |
| | PBE-D4 | -38.1 | -11.4 |
| | BP86-D3 | -37.4 | -10.7 |
| | BP86-D4 | -35.4 | -8.7 |
| | BLYP-D3 | -28.8 | -2.1 |
| | BLYP-D4 | -26.9 | -0.2 |
| Meta-GGA | TPSS-D3 | -34.9 | -8.1 |
| | M06L-D3 | -37.8 | -11.1 |
| Hybrid | B3LYP-D3 | -28.2 | -1.5 |
| | B3LYP-D4 | -26.2 | 0.5 |
| | PBE0-D3 | -34.1 | -7.4 |
| Meta-Hybrid | TPSSH-D3 | -33.1 | -6.4 |
| | M06-D3 | -34.8 | -8.1 |
| | M06-2x-D3 | -24.2 | 2.6 |
| range separate | CAM-B3LYP-D3 | -32.7 | -6.0 |
| | wB97X-D3 | -33.9 | -7.2 |
| | LC-BLYP-D3 | -49.2 | -22.5 |
| double-hybrid | PWPB95-D3 | -26.2 | 0.5 |
| | B2PLYP-D3 | -26.5 | 0.3 |
| Reference | CCSD(T) | -26.7 | |

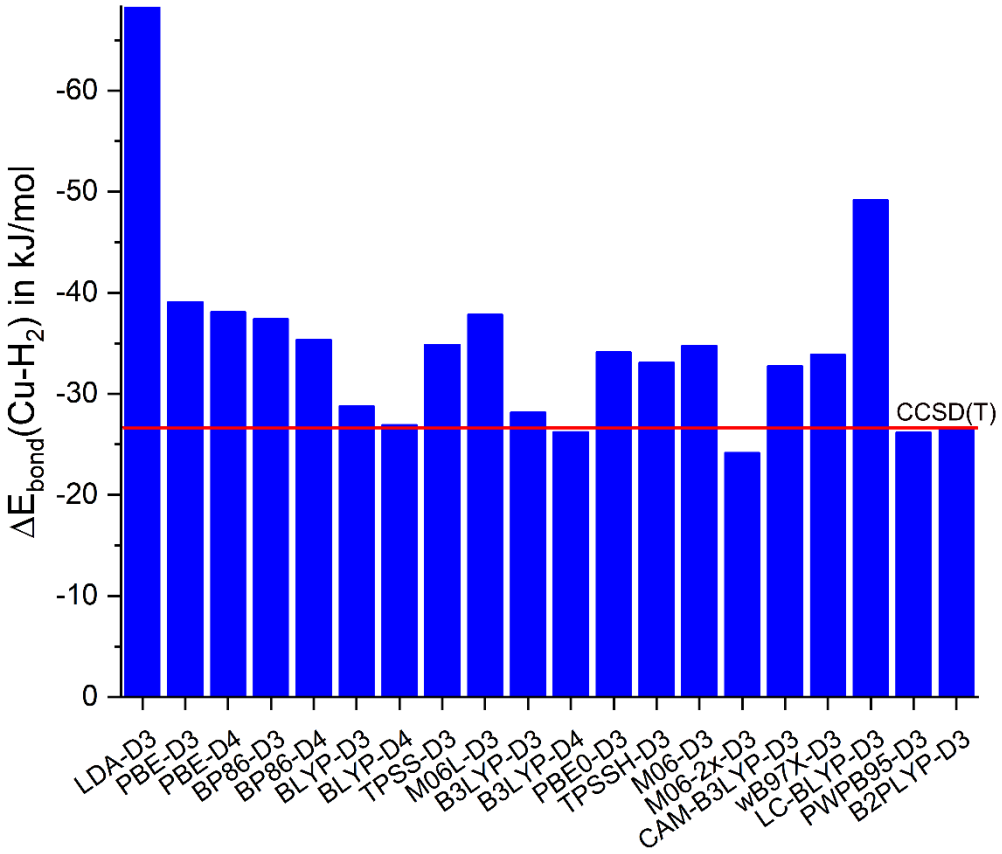


**Figure S7**: Bonding energy of Cu-$H_2$ bond in complex $Cu^+(H_2O)(H_2)_2$ in kJ/mol. The red line corresponds to CCSD(T) reference calculation.

The CCSD(T) results demonstrate deviations of less than 1 kJ·mol$^{-1}$ for the double hybrid functional, BLYP, and B3LYP with D4 dispersion correlation. Due to a missing implementation, double hybrid functionals cannot be utilized for Energy Decomposition Analysis (EDA) calculations. Therefore, B3LYP-D4 was selected for bond analysis.

**Stuctures**

For the EDA-NOCV (Energy Decomposition Analysis with Natural Orbital for Chemical Valence extension), all systems ($Cu(H_2)_4^+$, $Cu(H_2)_2(H_2O)^+$, $Cu(H_2)(H_2O)^+$, $Cu(H_2)^+$ and $Cu(H_2O)^+$) and fragments were optimized. The optimized structures of the studied complexes are shown in the **Figure S8**.

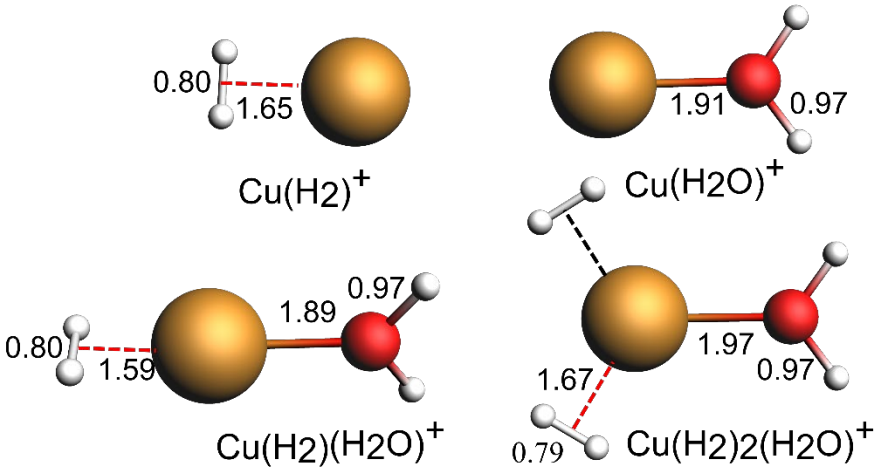


**Figure S8**: The optimized structure of the studied complexes, whereby all Cu–$H_2O$ and Cu–$H_2$ bonds (red) are analyzed by EDA. All bond lengths are in Å.

## Energy decomposition analysis with natural orbital for chemical valence (EDA-NOCV)

The settings for the EDA calculation are described in the methods section of the article. The EDA results are shown in **Table S15**.

**Table S15**: EDA result for Cu-$H_2O$ bond of $(Cu(H_2)_2(H_2O)^+$, $Cu(H_2)(H_2O)^+$ and $Cu(H_2O)^+$ and the Cu-O distance r(Cu-$H_2O$).[a]

| | $Cu(H_2)_2(H_2O)^+$ | | $Cu(H_2)(H_2O)^+$ | | $Cu(H_2O)^+$ | |
|---|---|---|---|---|---|---|
| $\Delta E_{int}$ | -162 | | -208 | | -190 | |
| $\Delta E_{int}$(disp)[b] | -6 | 4 % | -4 | 2 % | -4 | 2 % |
| $\Delta E_{int}$(elec)[b] | -156 | 96 % | -204 | 98 % | -186 | 98 % |
| $\Delta E_{elstat}$[c] | -226 | 68 % | -268 | 67 % | -273 | 66 % |
| $\Delta E_{Pauli}$ | 178 | | 196 | | 225 | |
| $\Delta E_{orb}$[c] | -107 | 32 % | -131 | 33 % | -137 | 34 % |
| $\Delta E_1$[d] | -62 | 58 % | -71 | 54 % | -73 | 53 % |
| $\Delta E_2$[d] | -16 | 15 % | -21 | 16 % | -29 | 21 % |

| | | | | | | |
|---|---|---|---|---|---|---|
| $\Delta E_3$[d] | -12 | 11 % | -16 | 12 % | -16 | 12 % |
| $\Delta E_3$[d] | -12 | 11 % | -16 | 12 % | -15 | 11 % |
| $\Delta E_{prep}$ | 25 | | 2 | | 1 | |
| $\Delta E_{prep}(H_2O)$ | 1 | | 1 | | 1 | |
| $\Delta E_{prep}(Cu^+L_{0\text{-}3})$ | 24 | | 1 | | 0 | |
| $\Delta E_{bond}$ | -137 | | -206 | | -189 | |
| $r(Cu-H_2O)$ | 1.97 | | 1.90 | | 1.91 | |

[a] All energies in kJ/mol, bond distances in Å computed with B3LYP-D4/TZ2P. Fragments are closed-shell species $Cu^+L_{0\text{-}3}$ and $H_2$ (L=$H_2O$, $H_2$) in Table S15 and $Cu^+L_{0\text{-}2}$ and $H_2O$ (L= $H_2$) in Table S16. [b] Percentage values give the relative contributions of dispersion and electronic effects to $\Delta E_{int}$. [c] Percentage values give the relative contributions to the attractive pEDA terms $\Delta E_{elstat}$ and $\Delta E_{orb}$. [d] Sum over all NOCV contributions corresponds to $\Delta E_{orb}$.

Bonding analysis of the $Cu^+$–$H_2O$ bond also shows a dative character for all $Cu(H_2O)(H_2)_n^+$ ($n$ = 0, 1, 2), in which the dispersion interaction makes only a small contribution (about -5 kJ·mol$^{-1}$). The $Cu^+$–$H_2O$ bond is about 100 kJ·mol$^{-1}$ stronger than the $Cu^+$–$H_2$ bond. Only complex $Cu(H_2O)(H_2)_2^+$ has a significant value for preparation energy due to the configuration change in the Cu fragment. Additionally the $Cu^+$–O bond distance for $Cu(H_2O)(H_2)_2^+$ is significantly larger than for the other two complexes correspond to a weaker interaction. For $Cu(H_2O)(H_2)^+$ and $Cu(H_2O)^+$, the Cu–O bond length is similar (1.90 Å and 1.91 Å, respectively). However, the interaction energy (and binding energy) is about 20 kJ·mol$^{-1}$ higher for $Cu(H_2)(H_2O)^+$ due to the significantly lower Pauli repulsion (30 kJ·mol$^{-1}$) for this complex, which explains the back bonding to the $H_2$ ligand. This reduces the electron density in the HOMO and HOMO-1, resulting in less repulsion with occupied orbitals of water. Orbital and electrostatic interactions are slightly stronger for $Cu(H_2O)^+$ (5 kJ·mol$^{-1}$ each). The weaker electrostatic and orbital interactions for $Cu(H_2)(H_2O)^+$ can be explained by the reduction of the charge at the Cu center due to the sigma donation of the LUMO by $H_2$ ligands.

**Figure S9** shows the four most important NOCVs for the Cu–$H_2O$ bonds. More than 90% of the $\Delta E_{orb}$ is accounted for by these NOCVs. The NOCVs for all investigated Cu–$H_2O$ bonds have the same shape but differ in their contributions to the $\Delta E_{orb}$ and the amount of charge transfer. All NOCV results indicate that there is a transfer of charge from the O atom in the water molecule to the Cu atom. Specifically, NOCV 1 represents the σ interaction between the free electron pair on

the O atom in the bonding direction and the empty s orbital on the Cu, while NOCV 2 represents the corresponding p orbital in the bonding direction of the Cu-atom. NOCV 4 shows the π interaction of the other free electron pair with the p orbital of the Cu atom. Finally, NOCV 3 describes the π interaction between the binding p orbital of the O atom in water and the last p orbital on the Cu.

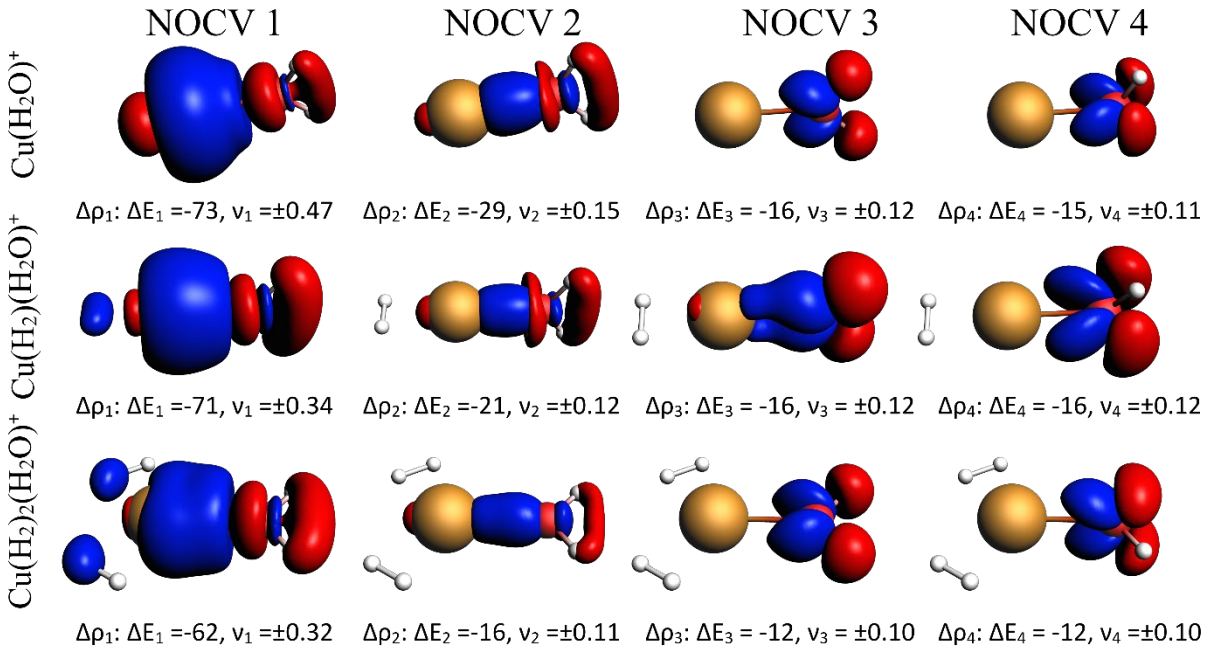


**Figure S11**: Selected deformation densities ($\Delta\rho_i$) from EDA-NOCVs for Cu-$H_2O$ bond with energy contribution ($\Delta E_i$) to $\Delta E_{orb}$ in kJ/mol and eigenvalues ($\nu_i$). Charge depletion (red) and charge accumulation (blue) with isosurface value 0.0020 for $Cu(H_2O)^+$, 0.0011 for $Cu(H_2)(H_2O)^+$ and 0.0015 for $Cu(H_2)_2(H_2O)^+$.


1 a) D. Sengupta, P. Melix, S. Bose, J. Duncan, X. Wang, M. R. Mian, K. O. Kirlikovali, F. Joodaki, T. Islamoglu, T. Yildirim, R. Q. Snurr and O. K. Farha, *J. Am. Chem. Soc.*, 2023, **145**, 20492; b) B. R. Barnett, H. A. Evans, G. M. Su, H. Z. H. Jiang, R. Chakraborty, D. Banyeretse, T. J. Hartman, M. B. Martinez, B. A. Trump, J. D. Tarver and others, *J. Am. Chem. Soc.*, 2021, **143**, 14884;

2 R. Xiong, L. Zhang, P. Li, W. Luo, T. Tang, B. Ao, G. Sang, C. Chen, X. Yan, J. Chen and M. Hirscher, *Chem. Eng. J.*, 2020, **391**, 123485.

3 B. Ipek, R. A. Pollock, C. M. Brown, D. Uner and R. F. Lobo, *J. Phys. Chem. C*, 2018, **122**, 540.

4 I. Weinrauch, I. Savchenko, D. Denysenko, S. M. Souliou, H.-H. Kim, M. Le Tacon, L. L. Daemen, Y. Cheng, A. Mavrandonakis, A. J. Ramirez-Cuesta, D. Volkmer, G. Schütz, M. Hirscher and T. Heine, *Nat. Commun.*, 2017, **8**, 14496.

5 J. Teufel, H. Oh, M. Hirscher, M. Wahiduzzaman, L. Zhechkov, A. Kuc, T. Heine, D. Denysenko and D. Volkmer, *Adv. Mater.*, 2013, **25**, 635.

6 H. Oh and M. Hirscher, *Eur. J. Inorg. Chem.*, 2016, **2016**, 4278.

7 T. Wulf and T. Heine, *Int. J. Quatum. Chem.*, 2018, **118**, e25545.

8 T. Wulf and T. Heine, *J. Phys. Chem. C*, 2020, **124**, 9409.

9 a) K. R. Asmis, A. Fielicke, G. von Helden and G. Meijer, in *Atomic clusters*, ed. D. Woodruff, Elsevier, Amsterdam and Boston, 2007, pp. 327–375; b) E. J. Bieske and O. Dopfer, *Chem. Rev.*, 2000, **100**, 3963; c) J. M. Lisy, *Int. Rev. Phys. Chem.*, 1997, **16**, 267; d) M. A. Duncan, *Int. Rev. Phys. Chem.*, 2003, **22**, 407; e) N. Heine and K. R. Asmis, *Int. Rev. Phys. Chem.*, 2015, **34**, 1;

10 a) G. Piccini and J. Sauer, *J. Chem. Theory. Comput.*, 2014, **10**, 2479; b) K. Sillar, A. Hofmann and J. Sauer, *J. Am. Chem. Soc.*, 2009, **131**, 4143;

11 a) F. Dahlmann, C. Lochmann, A. N. Marimuthu, M. Lara-Moreno, T. Stoecklin, P. Halvick, M. Raoult, O. Dulieu, R. Wild, S. Schlemmer and others, *J. Chem.Phys.*, 2021, **155**; b) F. Dahlmann, P. Jusko, M. Lara-Moreno, P. Halvick, A. N. Marimuthu, T. Michaelsen, R. Wild, K. Geistlinger, S. Schlemmer, T. Stoecklin, R. Wester and S. Brünken, *Mol. Phys.*, 2022, **120**;

12 J. Jin, T. Wulf, M. Jorewitz, T. Heine and K. R. Asmis, *Phys. Chem. Chem. Phys.*, 2023, **25**, 5262.

13 P. R. Kemper, P. Weis, M. T. Bowers and P. Ma\^\itre, *J. Am. Chem. Soc.*, 1998, **120**, 13494.

14 P. Maitre and C. W. Bauschlicher, *J. Phys. Chem.*, 1993, **97**, 11912.

15 a) R. H. Crabtree, *Chem. Rev.*, 2016, **116**, 8750; b) G. J. Kubas, *Metal dihydrogen and s-bond complexes: structure, theory, and reactivity*, Springer Science & Business Media, 2001;

16 N. Heine and K. R. Asmis, *Int. Rev. Phys. Chem.*, 2015, **34**, 1.

17 K. R. Asmis, M. Brümmer, C. Kaposta, G. Santambrogio, G. von Helden, G. Meijer, K. Rademann and L. Wöste, *Phys. Chem. Chem. Phys.*, 2002, **4**, 1101.

18 a) T. B. Ward, E. Miliordos, P. D. Carnegie, S. S. Xantheas and M. A. Duncan, *J. Chem.Phys.*, 2017, **146**, 224305; b) J. H. Marks, E. Miliordos and M. A. Duncan, *J. Chem.Phys.*, 2021, **154**, 64306; c) P. D. Carnegie, B. Bandyopadhyay and M. A. Duncan, *J. Chem.Phys.*, 2011, **134**;

19 P. D. Carnegie, McCoy, AB and M. A. Duncan, *J. Phys. Chem. A*, 2009, **113**, 4849.

20 T. Ziegler and A. Rauk, *Theoret. Chim. Acta*, 1977, **46**, 1.

21 K. Kitaura and K. Morokuma, *Int. J. Quatum. Chem.*, 1976, **10**, 325.

22 F. M. Bickelhaupt and E. J. Baerends, in *Reviews in Computational Chemistry*, ed. K. B. Lipkowitz and D. B. Boyd, Wiley, 2000, vol. 15, pp. 1–86.

23 L. Zhao, M. von Hopffgarten, D. M. Andrada and G. Frenking, *WIREs Comput. Mol. Sci.*, 2018, **8**.

24 M. P. Mitoraj, A. Michalak and T. Ziegler, *J. Chem. Theory. Comput.*, 2009, **5**, 962.

25 P. M. Morse, *Phys. Rev.*, 1929, **34**, 57.

26 M. Mayer and K. R. Asmis, *J. Phys. Chem. A*, 2021, **125**, 2801.

27 N. Heine and K. R. Asmis, *Int. Rev. Phys. Chem.*, 2016, **35**, 507.

28 J. F. Stanton, J. Gauss, L. Cheng, M. E. Harding, D. A. Matthews, and P. G. Szalay, Cfour.

29 M. J. Frisch, G. W. Trucks, H. B. Schlegel, G. E. Scuseria, M. A. Robb, J. R. Cheeseman, G. Scalmani, V. Barone, G. A. Petersson, H. Nakatsuji, X. Li, M. Caricato, A. Marenich, J. Bloino, B. G. Janesko, R. Gomperts, B. Mennucci, H. P. Hratchian, J. V. Ortiz, A. F. Izmaylov, J. L. Sonnenberg, D. W. Young, F. Ding, F. Lipparini, F. Egidi, J. Goings, B. Peng, A. Petrone, T. Henderson, D. Ranasinghe, V. G. Zakrzewski, J. Gao, N. Rega, G. Zheng, W. Liang, M. Hada, M. Ehara, K. Toyota, R. Fukuda, J. Hasegawa, M. Ishida, T. Nakajima, Y. Honda, O. Kitao, H. Nakai, T. Vreven, K. Throssell, J. A. Montgomery, J. E. Peralta, F. Ogliaro, M. Bearpark, J. J. Heyd, E. Brothers, K. N. Kudin, V. N. Staroverov, T. Keith, R. Kobayashi, J. Normand, K. Raghavachari, A. Rendell, J. C. Burant, S. S. Iyengar, J. Tomasi, M. Cossi, J. M. Millam, M. Klene, C. Adamo, R. Cammi, J. W. Ochterski, R. L. Martin, K. Morokuma, O.

Farkas, J. B. Foresman and D. J. Fox, Gaussian 16 (Revision C.01), Gaussian Inc., Wallingford CT, 2016.

30 T. Ziegler and A. Rauk, *Theoret. Chim. Acta*, 1977, **46**, 1.

31 G. te Velde, F. M. Bickelhaupt, E. J. Baerends, C. Fonseca Guerra, S. J. A. van Gisbergen, J. G. Snijders and T. Ziegler, *J. Comput. Chem.*, 2001, **22**, 931.

32 P. J. Stephens, F. J. Devlin, C. F. Chabalowski and M. J. Frisch, *The Journal of Physical Chemistry*, 1994, **98**, 11623.

33 E. Caldeweyher, S. Ehlert, A. Hansen, H. Neugebauer, S. Spicher, C. Bannwarth and S. Grimme, *The Journal of Chemical Physics*, 2019, **150**, 154122.

34 E. van Lenthe and E. J. Baerends, *J. Comput. Chem.*, 2003, **24**, 1142.

35 E. van Lenthe, A. Ehlers and E.-J. Baerends, *The Journal of Chemical Physics*, 1999, **110**, 8943.

36 a) A. D. Becke, *Phys. Rev. A*, 1988, **38**, 3098; b) J. P. Perdew, *Phys. Rev. B*, 1986, **33**, 8822;

37 J. P. Perdew, K. Burke and M. Ernzerhof, *Phys. Rev. Lett.*, 1996, **77**, 3865.

38 V. N. Staroverov, G. E. Scuseria, J. Tao and J. P. Perdew, *The Journal of Chemical Physics*, 2003, **119**, 12129.

39 Y. Zhao and D. G. Truhlar, *The Journal of Chemical Physics*, 2006, **125**, 194101.

40 Y. Zhao and D. G. Truhlar, *Theoret. Chim. Acta*, 2008, **120**, 215.

41 M. Ernzerhof and G. E. Scuseria, *The Journal of Chemical Physics*, 1999, **110**, 5029.

42 J. P. Perdew, J. Tao, V. N. Staroverov and G. E. Scuseria, *The Journal of Chemical Physics*, 2004, **120**, 6898.

43 T. Yanai, D. P. Tew and N. C. Handy, *Chemical Physics Letters*, 2004, **393**, 51.

44 Y.-S. Lin, G.-D. Li, S.-P. Mao and J.-D. Chai, *J. Chem. Theory. Comput.*, 2013, **9**, 263.

45 Y. Tawada, T. Tsuneda, S. Yanagisawa, T. Yanai and K. Hirao, *The Journal of Chemical Physics*, 2004, **120**, 8425.

46 L. Goerigk and S. Grimme, *J. Chem. Theory. Comput.*, 2011, **7**, 291.

47 S. Grimme, *The Journal of Chemical Physics*, 2006, **124**, 34108.

48 S. Grimme, J. Antony, S. Ehrlich and H. Krieg, *The Journal of Chemical Physics*, 2010, **132**, 154104.

49 E. Caldeweyher, J.-M. Mewes, S. Ehlert and S. Grimme, *Phys. Chem. Chem. Phys.*, 2020, **22**, 8499.

50 F. Neese, F. Wennmohs, U. Becker and C. Riplinger, *The Journal of Chemical Physics*, 2020, **152**, 224108.

51 F. Weigend and R. Ahlrichs, *Physical Chemistry Chemical Physics*, 2005, **7**, 3297.

52 a) E. J. Baerends, D. E. Ellis and P. Ros, *Chemical Physics*, 1973, **2**, 41; b) B. I. Dunlap, J. W. D. Connolly and J. R. Sabin, *The Journal of Chemical Physics*, 2008, **71**, 3396; c) K. Eichkorn, O. Treutler, H. Öhm, M. Häser and R. Ahlrichs, *Chemical Physics Letters*, 1995, **242**, 652; d) C. van Alsenoy, *J. Comput. Chem.*, 1988, **9**, 620;